Electrochimica Acta 54 (2009) 2877–2882

Contents lists available at ScienceDirect

Electrochimica Acta

journal homepage: www.elsevier.com/locate/electacta

Microwave assisted synthesis and electrochemical behaviour of $LiMg_{0.1}Co_{0.9}O_2$ for lithium rechargeable batteries

C.N. Zaheena [b], C. Nithya [a], R. Thirunakaran [a], A. Sivashanmugam [a], S. Gopukumar [a,*]

[a] Central Electrochemical Research Institute (CSIR), Karaikudi 630 006, Tamil Nadu, India
[b] Department of Chemistry, University of Calicut, Thenhippalam, Kerala, India

ARTICLE INFO

Article history:
Received 12 September 2008
Received in revised form 5 November 2008
Accepted 5 November 2008
Available online 17 November 2008

Keywords:
Cathode material
Charge/discharge
Layered oxide
Lithium battery
Microwave assisted solution technique

ABSTRACT

Layered $LiMg_{0.1}Co_{0.9}O_2$ has been synthesized using microwave assisted solution technique. The precursor has been subjected to thermo-gravimetric/differential thermal analysis (TG/DTA) and calcined at 850 °C. The precursor and the calcined powders were characterized by X-ray diffraction (XRD) to confirm the formation of single-phase layered material. Fourier transform infrared (FTIR) studies were carried out to understand the nature of the metal–ligand bond and the observations were consistent with the XRD spectrum. Scanning (SEM) and transmission electron microscope (TEM) images have been obtained to understand the surface morphology and the grain orientation of the synthesized material. Coin cells of 2016 type have been assembled using the synthesized layered material as the cathode active material, lithium foil as the counter and reference electrodes and 1 M $LiPF_6$ in 1:1 EC/DEC as the electrolyte. Coin cells were assembled and crimp sealed inside an argon filled glove box. The charge/discharge characteristics of the coin cells were evaluated galvanostatically in the potential range 2.7–4.3 V. Results indicate that $LiMg_{0.1}Co_{0.9}O_2$ delivers an average discharge capacity of ~135 mAh g^{-1} over the investigated 20 cycles and is a potential candidate for use as cathode material in lithium rechargeable cells.

1. Introduction

Advances in electrode active material play a critical role on the development of lithium-ion batteries. Among the several cathode materials, lithium transition metal oxides have shown attractive electrochemical performance in the applications involving lithium battery devices and they are utilized as positive electrodes due to their high redox potential and specific capacity during the lithium intercalation/deintercalation processes [1]. $LiCoO_2$ is the most preferred cathode active material as it is widely used in commercial lithium-ion batteries and was first reported as cathode active material by Misushima et al. [2]. It is well known that the practical capacity of $LiCoO_2$ is limited to around 140 mAh g^{-1} i.e., nearly half of its theoretical capacity (273 mAh g^{-1}). This material has an ordered rock salt structure (α-$NaFeO_2$ structure) and belongs to *R*3*m* space group. The high cost and toxicity of cobalt, however, makes the use of $LiCoO_2$ undesirable. In order to reduce the cost and to improve the cell voltage and specific capacity, attempts have been made to partially substitute cobalt with either transition metals or non-transition metals [3–5]. Recent attempts to improve the performance of $LiCoO_2$ by means of doping or coating have shown promising results for obtaining higher capacity with enhanced stability of the $LiCoO_2$ electrodes. Such modifications led to either improved capacity retention characteristics by suppressing the surface reactions of $LiCoO_2$ particles or higher achievable specific capacity by increasing the upper limit of the intercalation voltage through the formation of stronger M—O bonds and to stabilize the layered structure in its fully delithiated state [6]. Therefore, bulk doping and surface modification have been the strategies to improve the electrochemical performance of $LiCoO_2$ electrode. In this study, we present a microwave dielectric heating assisted solution method for the synthesis of $LiCoO_2$ and $LiMg_{0.1}Co_{0.9}O_2$ and their electrochemical performance.

2. Experimental

Fig. 1 shows the schematic flow chart of the synthesis procedure for $LiMg_{0.1}Co_{0.9}O_2$ using microwave assisted solution technique. Synthesis of $LiCoO_2$ and $LiMg_{0.1}Co_{0.9}O_2$, were carried out by mixing stoichiometric amounts of anhydrous $LiNO_3$ (Acros organics, India) and $Co(COOCH_3)_2{\cdot}4H_2O$ (Merck, India) with or without $Mg(NO_3)_2{\cdot}6H_2O$ (Merck, India) and dissolving in a minimum quantity of triple distilled water. The reagents were of 99% pure. The resulting metal ion solution was concentrated by stirring continuously under slightly warm condition (100 °C). The above concentrated pasty mass was transferred to a china dish and placed at the center of the rotating plate of microwave oven (Kenstar, India 2450 MHz, 800 W) and irradiated at 50% power. A portion of the

* Corresponding author. Fax: +91 4565 227779.
E-mail address: deepika_41@rediffmail.com (S. Gopukumar).

0013-4686/$ – see front matter © 2008 Elsevier Ltd. All rights reserved.
doi:10.1016/j.electacta.2008.11.009

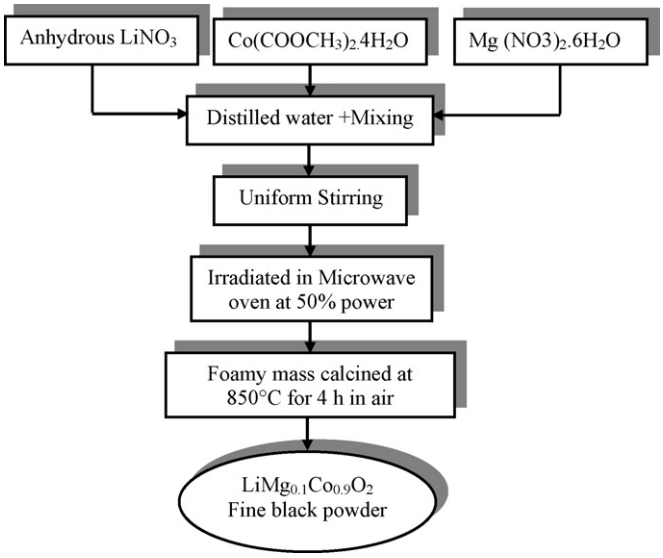

Fig. 1. Flow chart for the synthesis of $LiMg_{0.1}Co_{0.9}O_2$ by microwave assisted solution technique.

pasty mass was dried and taken for thermo-gravimetric/differential thermal analysis (TG/DTA) analysis. After the completion of irradiation the product was dried in an air oven. The resulting product was ground well to obtain a fine powder. Further, the powder was calcined at 850 °C for 4 h in air to obtain phase pure and highly crystalline $LiCoO_2$/$LiMg_{0.1}Co_{0.9}O_2$.

TG/DTA of the samples were examined under oxygen flow up to 850 °C at a heating rate of 10 °C min^{-1} to understand the thermal decomposition behaviour. The pre calcined and the calcined product were characterized by X-ray diffraction (XRD) ('Xpert PRO PAN alytical PW 3040/60 'X'Pert PRO') using Cu-Kα radiation (λ = 1.5418 Å), while the voltage and current were held at 40 kV and 20 mA (2θ = 0–80°) at a scan rate of 1° min^{-1}. The surface morphology and microstructure of synthesized samples were examined by scanning electron microscopy (SEM, HITACHI S–3000 H, Japan) and transmission electron microscopy (TEM, FEI-Tecnai-20 G2). FTIR spectra have been recorded on a Nicolet 5DX-FTIR spectroscope using KBr pellet in the range of 400–800 cm^{-1}.

The cathode was prepared by mixing 80 wt% of the active material, 10 wt% of acetylene black and 10 wt% of polyvinylidene fluoride (PVDF) binder in *N*-methylpyrrolidone (NMP) solvent to form homogeneous slurry. The slurry mixture was coated over an aluminium foil and dried under ambient condition. Circular electrodes of 18 mm diameter were blanked out and dried under vacuum at 120 °C for 12 h. Finally, coin cells of 2016 configuration were assembled in an argon filled glove box, in which lithium was used as the counter and reference electrode, celgard 2400 as the separator and $LiPF_6$ in 1:1 EC/DEC as the electrolyte. The charge–discharge studies of the coin cells were carried out in a programmable battery tester (BEATE, Germany) at C/20 rate for the first cycle and C/10 rate in the subsequent cycles between 2.7 and 4.3 V.

3. Results and discussion

3.1. TG/DTA

Fig. 2 shows the TG/DTA curves obtained for $LiCoO_2$ and $LiMg_{0.1}Co_{0.9}O_2$ powders obtained after the microwave irradiation. TG curves exhibit two significant weight loss regions. The first weight loss regions located from 152 to 261 °C (Fig. 2a) and 104 to 196 °C (Fig. 2b) for $LiCoO_2$ and $LiMg_{0.1}Co_{0.9}O_2$ respectively could be ascribed to the loss of superficial or absorbed water. The weight loss region observed from 261 to 412 °C (Fig. 2a) and 196 to 267 °C (Fig. 2b) for $LiCoO_2$ and $LiMg_{0.1}Co_{0.9}O_2$ respectively can be assigned to the decomposition of the nitrate and acetate precursor materials. DTA curves involve exothermic peaks centered at 401 °C (Fig. 2a) and 262 °C (Fig. 2b) and can be associated with the formation of $LiCoO_2$ and $LiMg_{0.1}Co_{0.9}O_2$ material respectively. It is interesting to observe that the formation temperature is significantly reduced by the addition of $Mg(NO_3)_2$ indicating better combustion and involving lesser processing time. This fact is supplemented by XRD spectrum (Fig. 3a) obtained for the precursors before calcination at 850 °C wherein all the signature peaks corresponding to the layered $LiCoO_2$ are present with few additional peaks. Further, the appearance of slightly broad nature of the peaks counsel that the material needs a subsequent calcination step for the structural refinement in order to obtain a highly crystalline product.

3.2. X-ray diffraction

Fig. 3a and b shows the XRD patterns of $LiCoO_2$ and $LiMg_{0.1}Co_{0.9}O_2$ powders before and after calcination respectively at 850 °C. The XRD patterns of the samples before calcination confirm the formation of layered material as they exhibit all the signature peaks corresponding to that of $LiCoO_2$ (JCPDS card no.: 44-0145) as a low intensity and fairly broad reflections. Further, the XRD pattern of $LiMg_{0.1}Co_{0.9}O_2$ exhibits impurity peaks (marked with *) around diffraction angles 31° and 44° may be attributed to traces of MgO. It is apparent that such impurity peaks are not observed

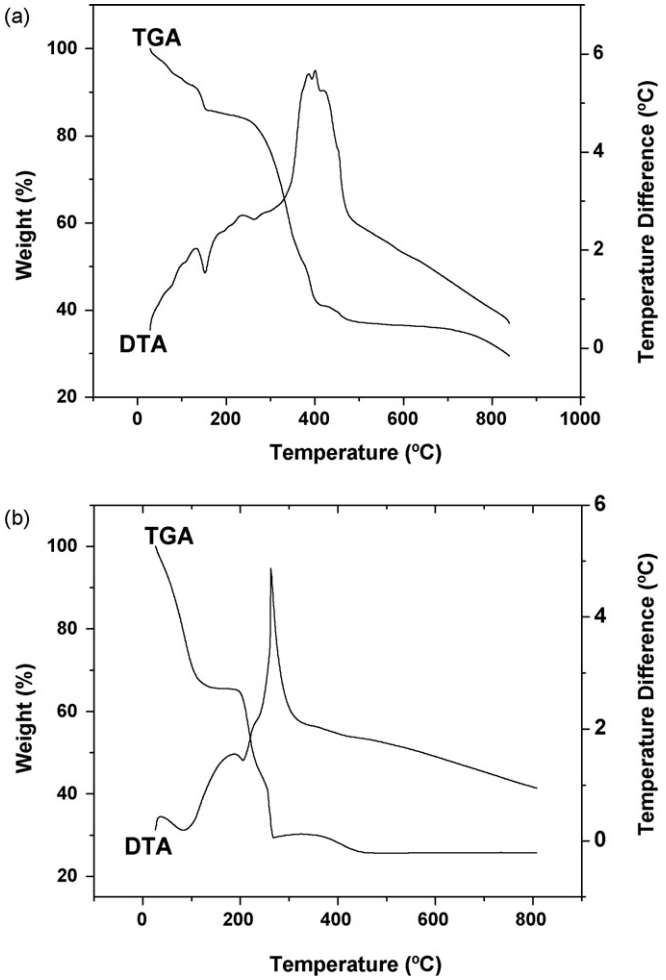

Fig. 2. TG–DTA curves of (a) $LiCoO_2$ (b) $LiMg_{0.1}Co_{0.9}O_2$ precursors.

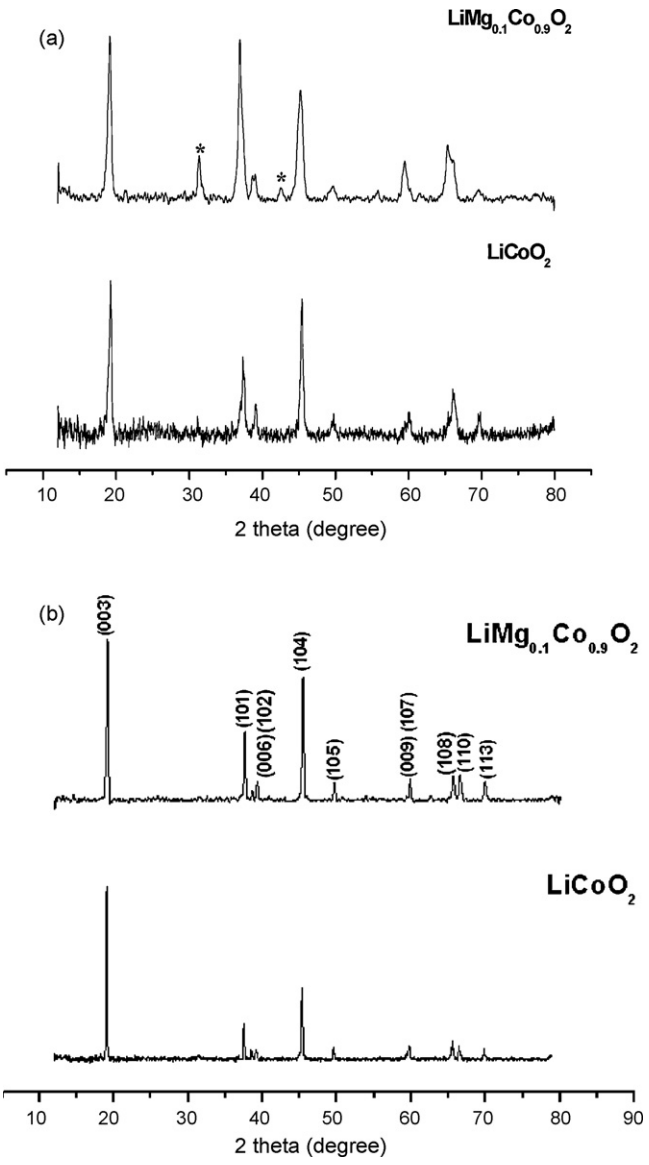

Fig. 3. X-ray diffraction patterns of microwave irradiated $LiCoO_2$ and $LiMg_{0.1}Co_{0.9}O_2$ particles (a) without calcination (b) calcined at 850 °C.

with $LiCoO_2$. These observations enlighten the fact that the material obtained after the microwave irradiation is of poor crystalline in nature and need further structural refinement. However, in the case of XRD patterns for the $LiCoO_2$ and $LiMg_{0.1}Co_{0.9}O_2$ samples calcined at 850 °C (Fig. 3b) the presence of high intensity reflections are assignable to a highly crystalline and phase pure layered material as there were no impurity peaks and the peak signatures could be indexed to α-$NaFeO_2$ layered structure with *R*3*m* space group and is free from Li_2CO_3, Co_3O_4 phases, whose intensity peaks are expected at around 31.797° and 36.853° [7]. The appearance of doublets at planes 0 0 6/1 0 2 and 1 0 8/1 1 0 indicate the stabilization of two-dimensional structure and an ordered distribution of lithium and cobalt ions in the inner lattice [8]. The lattice constants '*a*' and '*c*' were calculated using unit cell software package and the cell parameters along with the estimated standard deviations are tabulated (Table 1) The lattice constants $a = 2.8119$ Å; $c = 14.0321$ Å for $LiCoO_2$ and $a = 2.8119$ Å; $c = 14.0695$ Å for $LiMg_{0.1}Co_{0.9}O_2$ were obtained from least square plots with 0.0007 and 0.0056 as estimated standard deviation. It can be seen that, there is only change in '*c*' parameter suggesting that the small amounts of Mg-doping in $LiMg_{0.1}Co_{0.9}O_2$ has no influence over '*a*' values [9,10] and the expansion in *c*-direction is attributed to a low degree of cation mixing [11] i.e., Li/Co ordering and Mg/Co disordering. However, this kind of structural vacillation is found to be beneficial for Li ion insertion and extraction. Hence, Mg^{2+} is found to have a positive effect towards the positive structural modification of $LiCoO_2$.

Table 1
Unit cell parameters.

Unit cell parameter	$LiCoO_2$	Standard deviation	$LiMg_{0.1}Co_{0.9}O_2$	Standard deviation
a	2.8119	0.0007	2.8119	0.0007
c	14.0321	0.0056	14.0695	0.0332

3.3. Scanning electron microscopy

SEM micrographs of $LiCoO_2$ and $LiMg_{0.1}Co_{0.9}O_2$ calcined at 850 °C are presented in Fig. 4a and b respectively. The particles are found to be crystalline with well-defined facets that have a wide range of distribution ranging from 0.5 to 1 μm. However, in the case of $LiMg_{0.1}Co_{0.9}O_2$ (Fig. 4b) the particles are smaller and agglomerated as compared to $LiCoO_2$.

3.4. Transmission electron microscopy

Typical TEM images of the $LiCoO_2$ and $LiMg_{0.1}Co_{0.9}O_2$ calcined at 850 °C are also shown in Fig. 5a and b respectively. It can be seen that the particles are of cubical morphology with clear grain boundaries for both the materials. The insets in the figures indicate the selected area electron diffraction (SAED) pattern of the samples. The pres-

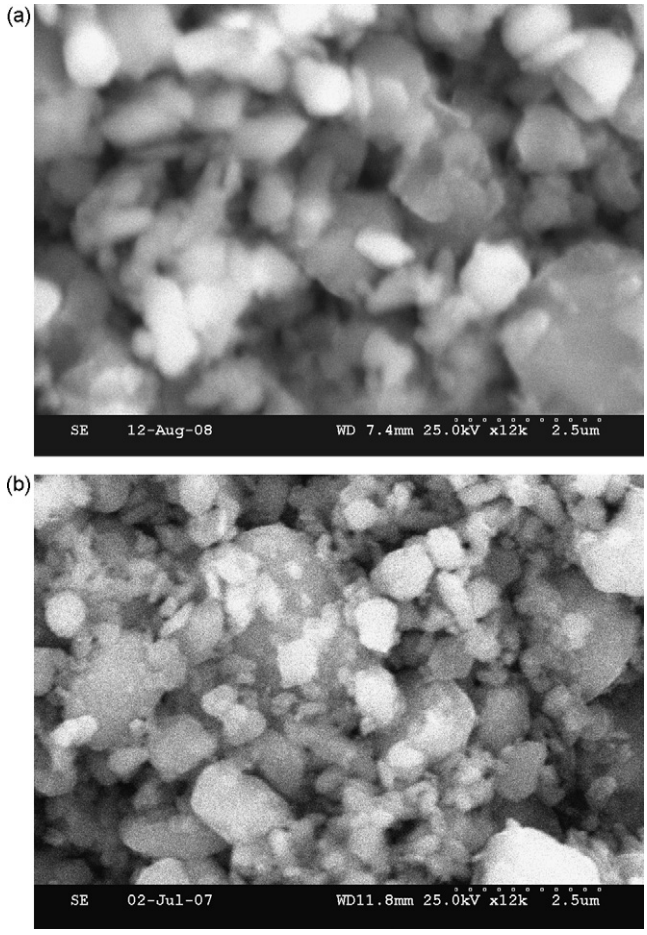

Fig. 4. SEM images of (a) $LiCoO_2$ (b) $LiMg_{0.1}Co_{0.9}O_2$ particles calcined at 850 °C.

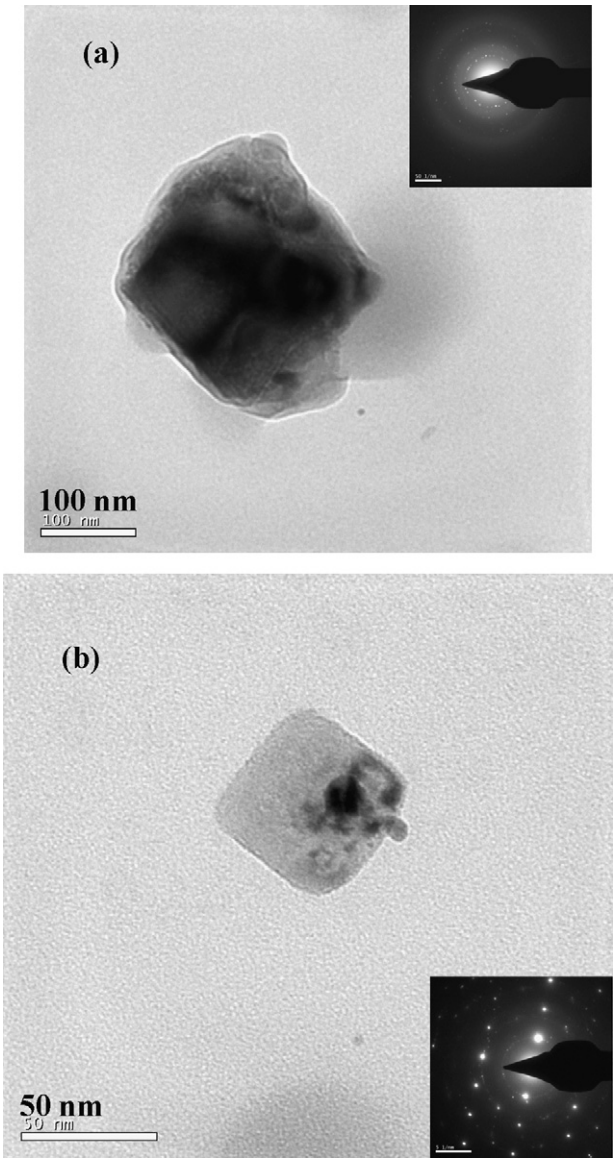

Fig. 5. TEM images of (a) $LiCoO_2$ (b) $LiMg_{0.1}Co_{0.9}O_2$ particles calcined at 850 °C.

ence of a diffused hollow with vaguely appearing rings and dots in the SAED pattern corroborate the low order crystalline behaviour of $LiCoO_2$. However, the appearance of clear and intense rings and dots without a diffused hollow in the SAED patterns of $LiMg_{0.1}Co_{0.9}O_2$ confirms the high crystalline nature [12]. The average grain size of the particles is around ~150 nm in the case of $LiCoO_2$ and ~50 nm for $LiMg_{0.1}Co_{0.9}O_2$.

3.5. FTIR

Fig. 6a and b depicts the FTIR spectra of microwave irradiated $LiCoO_2$ and $LiMg_{0.1}Co_{0.9}O_2$ particles without calcination and the calcined samples at 850 °C respectively. The spectra of the samples without calcination contain the reflections for Li–O and Co–O bands less defined due to poor crystalline nature of the material. However, when they are calcined at 850 °C the Co–O (660 cm^{-1}) in Co_3O_4 stretching frequency [13] disappears and the characteristic bands pertaining to $LiCoO_2$ and $LiMg_{0.1}Co_{0.9}O_2$ are observed. The characteristic stretching vibrations of Co–O (560 and 601 cm^{-1}) [14,15] and Mg–O (640 cm^{-1}) [16] are also observed. The Li–O stretching at 536 cm^{-1} is similar to the one observed for layered $LiCoO_2$ [17–20].

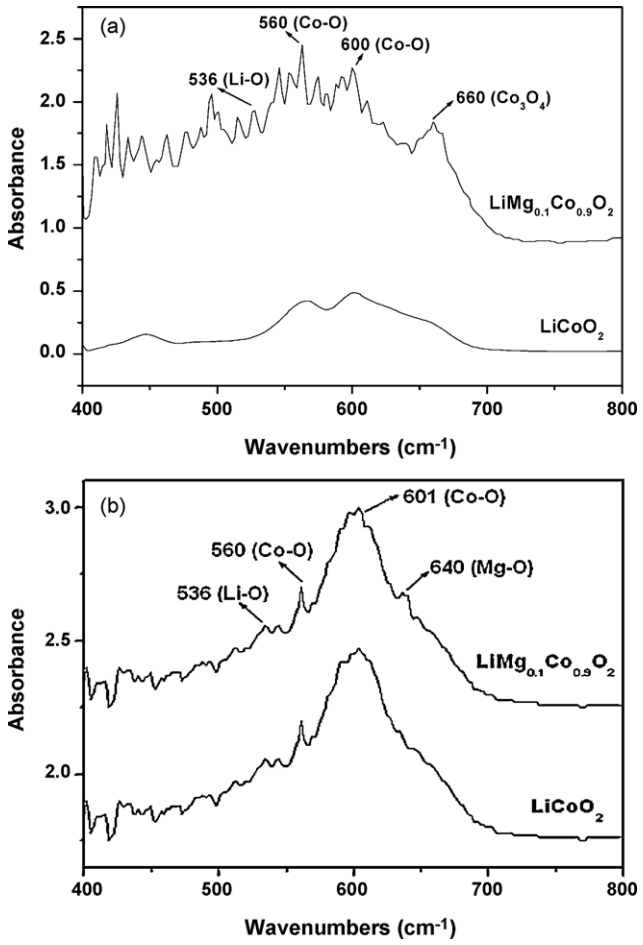

Fig. 6. FTIR spectra of microwave irradiated $LiCoO_2$ and $LiMg_{0.1}Co_{0.9}O_2$ particles (a) without calcination (b) calcined at 850 °C.

These data indicate the formation of compressed CoO_6 and LiO_6 octahedra. The intensity of the stretching mode increases significantly for $LiMg_{0.1}Co_{0.9}O_2$ and compares with the shape of IR at 510–570 cm^{-1} for α-$LiAlO_2$. These results show that the doping with Mg is not affecting the local environment of Li ions surrounded by oxygen anions and the covalence of CoO_2 layer increases marginally [21].

3.6. Charge–discharge studies

Electrochemical characterization was carried out by galvanostatic charge–discharge cycling studies between 2.9 and 4.3 V at C/20 rate for the first cycle and C/10 rate for the subsequent cycles. Fig. 7 shows the first charge–discharge curves of $LiCoO_2$ and $LiMg_{0.1}Co_{0.9}O_2$. It is observed that Mg-doping increases the charge capacity from 165 to 190 mAh g^{-1} and the discharge capacity from 125 to 146 mAh g^{-1}. The increase of discharge capacity can be ascribed to the occupancy of Mg^{2+} ions in the inter-slab space along with Co^{3+} ions which facilitates the transit of Li^+ ions above 4.2 V. The relatively larger ionic radius of Mg^{2+} ion (0.72 Å) than that of the Co^{3+} ion (0.63 Å) allow free movement of Li^+ ions due to pillaring effect [22,23] and also prevent the vacancy ordering. This fact is corroborated from the marginal increase observed in the 'c' lattice (Table 1). As the charge–discharge proceeds the dopant ions located on the electrode surface form a solid solution with Co^{4+} ions. This solid solution acts as an intermediate layer and minimizes the dissolution of Co^{4+} ions into the electrolyte. This phase formation stabilizes the structure and enhances the cycle stability

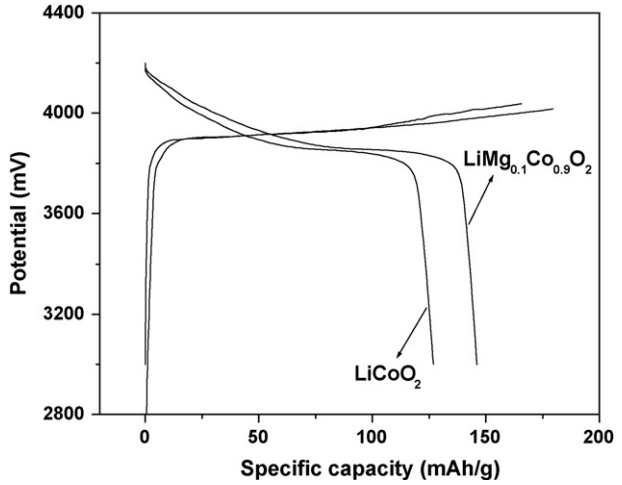

Fig. 7. Galvanostatic first cycle charge/discharge curves of $LiCoO_2$ and $LiMg_{0.1}Co_{0.9}O_2$ at C/10 rate.

up to 4.2 V [22]. Nevertheless, the morphology and the nano sized (~50 nm) particles of the Mg-doped $LiCoO_2$ also supplement the high discharge capacity as it obviously provides shorter diffusion path lengths for lithium-ion transport.

Furthermore, the flat plateau potential present at the end of the discharge cycle is attributed to the existence of two discrete crystalline phases with different Li contents as reported by Ohzuku [23]. Doping of Mg^{2+} in $LiCoO_2$ enhances the conductivity of $LiCoO_2$ as well as its structural stability as it creates more Co^{4+} ions due to charge compensation. Subsequently, Li^+ vacancies are generated to balance the excess covalence greatly increase the conductivity of $LiCoO_2$ and thereby enhance the electrochemical performance [24].

Fig. 8 depicts the cycling performance of the pristine $LiCoO_2$ and Mg-doped $LiCoO_2$ electrodes for the investigated 20 cycles. Mg-doped sample exhibits better capacity retention than the bare $LiCoO_2$. In the case of $LiMg_{0.1}Co_{0.9}O_2$, the first discharge capacity is as high as 146 mAh g^{-1} and at the end of 20th cycle the capacity is 125 mAh g^{-1}. It is interesting to note that there is only 13% decrease in capacity at the end of 20th cycle which is less than that reported by several authors [25–30]. The superior performance of $LiMg_{0.1}Co_{0.9}O_2$ could be attributed to Mg-doping as it leads to the simultaneous presence of Co^{4+} ions and to a smaller extent of intermediated spin $Co^{3+(1S)}$ ions both contributing to an enhanced conductivity as compared to that of undoped [10].

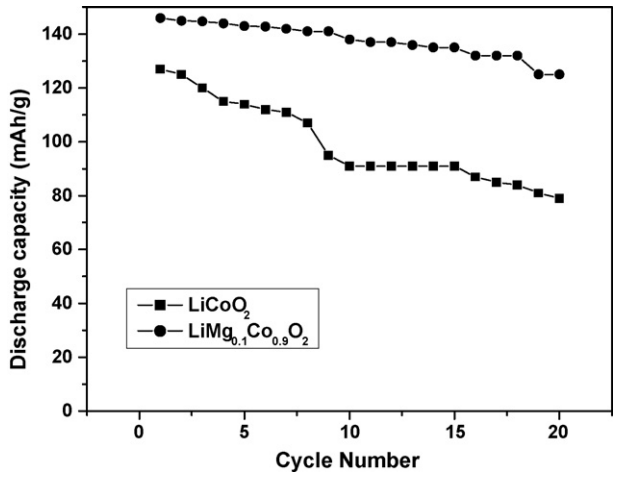

Fig. 8. Discharge capacity vs. cycle number curves of $LiCoO_2$ and $LiMg_{0.1}Co_{0.9}O_2$ at C/10 rate.

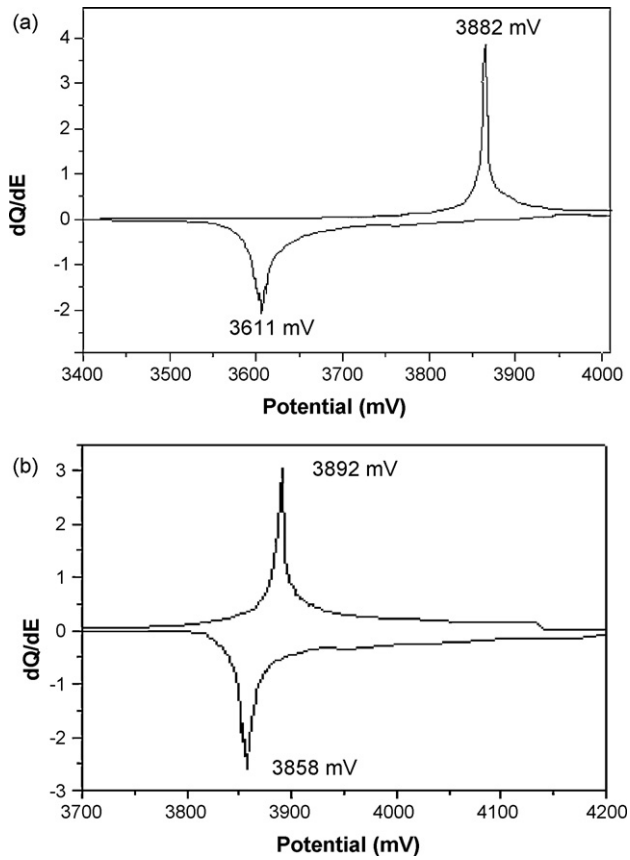

Fig. 9. dQ/dE vs. potential curves of (a) $LiCoO_2$ (b) $LiMg_{0.1}Co_{0.9}O_2$.

Therefore, Mg-doped $LiCoO_2$ synthesized by microwave assisted solution method with subsequent calcination exhibits better capacity retention characteristics in the present case when compared to previously reported microwave method without calcination [31] and other synthesis routes [32–34].

3.7. Differential capacity curves

Fig. 9a and b represents the dQ/dE vs. potential curves for the bare $LiCoO_2$ and $LiMg_{0.1}Co_{0.9}O_2$ respectively. The differential capacity curves of $LiMg_{0.1}Co_{0.9}O_2$ for the charge–discharge profiles exhibit symmetrical and sharp intensity reflections than that of bare $LiCoO_2$ indicating the facile lithium-ion diffusion. Furthermore, in the case of $LiMg_{0.1}Co_{0.9}O_2$ the potential separation between anodic and cathodic peaks is only 34 mV, whereas it is 271 mV for the bare $LiCoO_2$. The well-defined peaks and narrower peak separation in the case of $LiMg_{0.1}Co_{0.9}O_2$ suggest that the reversibility of the electrode reaction is markedly enhanced by Mg-doping. This fact is demonstrated by the enhanced cycling stability of $LiMg_{0.1}Co_{0.9}O_2$ material [35–37].

4. Conclusions

Mg-doped $LiCoO_2$ has been successfully synthesized by microwave assisted solution technique. Microscopy studies reveal that the particle size is around 50–100 nm. XRD patterns suggest that Mg-doping favours the formation of highly refined crystals of layered structure with marginally expanded 'c' lattice thereby providing more space for lithium-ion intercalation/deintercalation. In addition, the doping enhances the conductivity thereby improving the reversibility of the electrode reaction. $LiMg_{0.1}Co_{0.9}O_2$ deliver an average discharge capacity of around 135 mAh g^{-1} suggest-

ing that Mg-doping enhances the electrochemical performance of $LiCoO_2$.

References

[1] T. Ohzuku, A. Ueda, Solid-State Ionics 69 (1994) 201.
[2] K. Misushima, P.C. Jones, P.J. Wiseman, J.B. Goodenough, Mater. Res. Bull. 15 (1980) 783.
[3] C. Delmas, I. Saadoune, A. Rougier, J. Power Sources 43–44 (1993) 595.
[4] K.K. Lee, K.B. Kim, J. Electrochem. Soc. 147 (2000) 1709.
[5] C. Delams, I. Saadoune, Solid-State Ionics 53–56 (1992) 370.
[6] Z.X. Wang, L.J. Liu, L.Q. Chen, X.J. Huang, Solid-State Ionics 148 (2002) 335.
[7] S.M. Lala, L.A. Montoro, V. Lemos, M. Abbate, J.M. Rosolen, Electrochim. Acta 51 (2005) 7.
[8] H.Y. Xu, S. Xie, C.P. Zhang, C.H. Chen, J. Power Sources 148 (2005) 90.
[9] R. Thirunakaran, N. Kalaiselvi, P. Periasamy, N.G. Renganathan, Ionics 9 (2003) 388.
[10] S. Levasseur, M. Menetrier, C. Delmas, Chem. Mater. 14 (2002) 3584.
[11] Yuan Gao, M.V. Yakovlena, W.B. Ebner, Electrochem. Solid-State Lett. 1 (3) (1998) 117.
[12] Y. Zhang, C.Y. Chung, L.X. Sun, M. Zhu, Mater. Chem. Phys. 107 (2008) 254.
[13] Y. Bai, H. Shi, Z. Wang, L. Chan, J. Power Sources 167 (2007) 504.
[14] Y. Gu, D. Chen, X. Jian, J. Phys. Chem. B 109 (2005) 17901.
[15] C. Julien, L. El-Farh, S. Rangan, M. Massot, J. Sol–gel Sci. Technol. 15 (1999) 63.
[16] P.B. Balbuena, Y. Wang (Eds.), Lithium-Ion Batteries: Solid-Electrolyte Interphase, Imperial College Press, 2004, p. 176.
[17] W. Huang, R. Frech, Solid State Ionics 86–88 (1996) 395.
[18] T.A. Hewston, B.L. Chamberland, J. Phys. Chem. Solids 48 (1987) 97.
[19] T. Ohzuku, A. Ueda, M. Nagayama, Y. Iwakoshi, H. Komori, Electrochim. Acta 38 (1993) 1159.
[20] T.F. Yi, Y.R. Zhu, Electrochim. Acta 53 (2008) 3120.
[21] A. Amdouni, H. Zarrouk, F. Soulette, C. Julien, Mater. Chem. Phys. 80 (2003) 205.
[22] H.S. Kim, T.K. Ko, B.K. Na, W.I. Cho, B.W. Chao, J. Power Sources 138 (2004) 232.
[23] T. Ohzuku, A. Ueda, J. Electrochem. Soc. 141 (1994) 2972.
[24] F. Nobili, F. Croce, B. Scrosati, R. Marassi, Chem. Mater. 13 (2001) 1642.
[25] H. Tukamato, A.R. West, J. Electrochem. Soc. 144 (1997) 3164.
[26] S. Rodrigues, N. Munichandraiah, A.K. Shukla, J. Power Sources 102 (2001) 322.
[27] S. Gopukumar, Y. Jeong, K.B. Kim, Solid-State Ionics 159 (2003) 223.
[28] C. Julien, M.A. Camcho-Lopez, T. Mohan, S. Chitra, P. Kalyani, S. Gopukumar, Solid-State Ionics 135 (2000) 241.
[29] G.T.K. Fey, P. Muralidharan, C.Z. Lu, Y.D. Cho, Electrochim. Acta 51 (2006) 4850.
[30] H. Wook, N.J. Yun, M.H. Kim, M.H. Woo, K. Kim, Electrochim. Acta 51 (2006) 3297.
[31] P. Elumalai, H.N. Vasan, N. Munichandraiah, J. Power Sources 125 (2004) 77.
[32] H.J. Kim, Y.U. Jeong, J.H. Lee, J.J. Kim, J. Power Sources 159 (2006) 233.
[33] S. Frangini, S. Scaccid, M. Carewska, Electrochim. Acta 48 (2003) 3473.
[34] S. Levasseur, M. Menetrier, C. Delmas, J. Power Sources 112 (2002) 419.
[35] Z. Chen, J.R. Dahn, Electrochim. Acta 49 (2004) 1073.
[36] S. Madhavi, G.V. Subba Rao, B.V.R. Chowdari, S.F.Y. Li, Electrochim. Acta 48 (2002) 219.
[37] Y.J. Kim, H. Kim, B. Kim, D. Ahn, J.G. Lee, T.J. Kim, D. Son, J. Cho, Y.W. Kim, B. Park, Chem. Mater. 15 (2003) 1505.